Heliyon

ELSEVIER

Received:
14 October 2015
Revised:
31 December 2015
Accepted:
22 January 2016

Heliyon (2016) e00072

Performance evaluation of nanoclay enriched anti-microbial hydrogels for biomedical applications

Sonali Karnik [a,1], **Udayabhanu M. Jammalamadaka** [a,1], **Karthik K. Tappa** [a,1], **Rebecca Giorno** [b], **David K. Mills** [a,b,*]

[a] *Department of Biomedical Engineering, Louisiana Tech University, Ruston, LA, USA*

[b] *School of Biological Sciences, Louisiana Tech University, Ruston, LA, USA*

* Corresponding author at: Center for Biomedical Engineering and Rehabilitation Sciences and School of Biological Sciences, Louisiana Tech University, Carson Taylor Hall, Room 128, Ruston, LA, USA.
E-mail address: dkmills@latech.edu (D.K. Mills).

[1] These authors contributed equally to this work.

Abstract

A major factor contributing to the failure of orthopedic and orthodontic implants is post-surgical infection. Coating metallic implant surfaces with anti-microbial agents has shown promise but does not always prevent the formation of bacterial biofilms. Furthermore, breakdown of these coatings within the human body can cause release of the anti-microbial drugs in an uncontrolled or unpredictable fashion. In this study, we used a calcium alginate and calcium phosphate cement (CPC) hydrogel composite as the base material and enriched these hydrogels with the anti-microbial drug, gentamicin sulfate, loaded within a halloysite nanotubes (HNTs). Our results demonstrate a sustained and extended release of gentamicin from hydrogels enriched with the gentamicin-loaded HNTs. When tested against the gram-negative bacteria, the hydrogel/nanoclay composites showed a pronounced zone of inhibition suggesting that anti-microbial doped nanoclay enriched hydrogels can prevent the growth of bacteria. The release of gentamicin sulfate for a period of five days from the nanoclay-enriched hydrogels would supply anti-microbial agents in a sustained and controlled manner and assist in preventing microbial growth and biofilm formation on the titanium implant

http://dx.doi.org/10.1016/j.heliyon.2016.e00072

surface. A pilot study, using mouse osteoblasts, confirmed that the nanoclay enriched surfaces are also cell supportive as osteoblasts readily, proliferated and produced a type I collagen and proteoglycan matrix.

Keywords: Health sciences, Engineering, Biological sciences, Bioengineering, Biomedical engineering, Biomaterials

1. Introduction

Dental and orthopedic appliances, devices, and implants (hereafter collectively termed 'implants') have been in widespread use for over fifty years [1,2, 3]. Advances in surgical techniques and population longevity have drastically increased both the need and demand for dental and orthopedic procedures worldwide [4]. Dental and orthopedic complaints (dysfunction, impairment, pain) are the major reason that most Americans seek clinical intervention. In the United States alone, more than half a million people undergo total joint replacement each year and over 50 million yearly receive some form of dental or orthopedic device or implant. Worldwide, total joint replacements have been estimated at 959,000 annually, including both primary and revision total hip replacement procedures [5].

Titanium is the most frequently used metal in dental and orthopedic implants due to its tensile strength, biocompatibility and corrosion resistance [6, 7, 8, 9, 10]. In an ideal situation, the implant is accepted by and integrated into the surrounding native tissue resulting in a healthy functioning joint. Bacterial adsorption and surface colonization of the implant surface [11, 12] and failure of the implant to integrate with surrounding tissues [11, 12, 13] are the leading cause of implant failure as well as the resulting *sequela* that affects a patient's recovery. Resolving an implant infection usually requires that the implant be entirely removed, surrounding tissue cleaned of infection, and then a second prosthetic device is implanted. Revision arthroplasties and increased hospital stays can cost hundreds of thousands of dollars for a single patient. There are additional drawbacks to replacement surgeries including: inferior recovery compared to the initial surgery, further postsurgical complications and pain, reduced host defense, significant lost time from work, altered and restricted lifestyles, and even death. Current statistics indicate that infection is responsible for causing implant failure in approximately 1% of hip implants, 4% of knee implants, and more than 15% of implants associated with orthopedic trauma, where the wounds are deep, often filled with debris, such as seen in accident or battlefield injuries [14, 15].

In their original design, titanium implants were designed simply as mechanical devices; the biological aspects of the implant were a byproduct of stable internal or external device fixation to surrounding bone or soft tissue [16]. Surface

http://dx.doi.org/10.1016/j.heliyon.2016.e00072

adsorption of serum proteins facilitates bacterial adhesion and proliferation on the implant surface leading to biofilm formation [11, 17]. A biofilm is a multicellular community of microbes that forms on a solid surface or at a liquid–air interface [18, 19]. In a biofilm, microbes are densely packed within a self-assembled extracellular matrix (ECM) that provides protection for resident bacteria from various environmental agents. This ECM makes embedded bacteria more resistant to antibiotics than the resident bacteria normally present in the human body [10]. Often this can lead to the development of a very resistant biofilm that may increase bacterial pathogenicity and is the major reason that biofilm formation is responsible for a host of periprosthetic infections (PPIs) [20]. PPIs occur in approximately 1% to 2% of primary arthroplasties [21, 22] and can be greater than 10% in secondary arthroplasties [23, 24].

A common regimen for patients suffering from PPI is multiple surgeries (wound debridement) and an extended period of antibiotic therapy resulting in suffering and further disability [1, 25]. To reduce complications from PPI, delivering antibiotics directly to the implant site rather then systemically through intravenous injection and/or oral drugs could reduce the outbreak of toxic bacterial strains such as *C. difficile.* To control post-surgical infection of commercial implants, many manufacturers have used antibiotic and silver adsorption [26, 27] anti-bacterial coatings [28, 29, 30] impregnation [21] or limited anodization with silver impregnation [13]. However, the release of anti-bacterial and anti-fungals are short-lived and result in less than maximal antibiotic release or microbial growth inhibition. Most of these surface modification methods have failed primarily due to their inability to provide sustained antibacterial effects due to rapid dissolution from the implant microenvironment. The quick (and excessive) release of antimicrobials also raises a major health concern as assisting in the growing emergence of antibiotic/fungal resistant strains [31, 32, 33].

Recently, nanoporous titanium has emerged as a potential nanostructured surface. It has a low elastic modulus and a nanotopography that can be tailored to specific dimensions [34, 35, 36]. Through anodization, the nanoporous surface can be controlled to specific dimensions that promote cytocompatibility and tissue integration of dental implant surface coatings and orthopedic implants [37, 38]. Moreover, the nanotube titanium surface can be used to store and then release a suite of bioactive agents. In this study, titanium, was anodized to produce nanoporous titanium (NPT) and modified into an anti-infective hydrogel surface coating. Hydrogel coatings consisted of alginate with calcium phosphate cement (CPC) and/or chitosan and enhanced with halloysite nanotubes (HNTs) loaded with an anti-bacterial drug, Gentamicin. The anodized surface of the titanium would be favorable for the growth of eukaryotic cells and the bacterial growth would be prevented. Halloysite is chemically an aluminosilicate and

http://dx.doi.org/10.1016/j.heliyon.2016.e00072

upon hydration rolls up to form nanotubes with an average length ranging from 1–3 μm and average diameter ranging in 30–70 nm [57, 58]. Use of HNTs as drug carriers and delivery vehicles for bioactive molecules has been studied and the release of these molecules form HNTs is sustained [46, 47, 48, 49, 51, 54]. Gentamicin is a heat stable antibiotic used widely in orthopedic surgeries and is effective against gram-negative bacteria [39]. Gentamicin doped hydrogels were found to have a sustained release of gentamicin that inhibited the growth of *E. coli* bacteria. A pilot study using mouse pre-osteoblasts confirmed that the hydrogel coatings were cell supportive. The graphical representation of the titanium-hydrogel composite in Fig. 1 illustrates our concept of an anodized titanium with an anti-microbial hydrogel coating.

The titanium metal (T) is anodized on the surface to produce a rough and featured topography (AT). Hydrogel coating (H) which is composed of anti-microbial agent, Gentamicin, (G) loaded HNTs is coated on to the anodized surface of the titanium to prevent bacterial (B) attachment and biofilm formation. Gentamicin will be released in a sustained manner over an extended period of time preventing the bacteria to grow of the metal implant surface.

2. Experimental

2.1. Materials

Unless otherwise stated, all chemicals for synthesis and physicochemical analysis were of ACS grade, purchased from Sigma-Aldrich and used as received without further purification. Gentamicin sulfate antimicrobial susceptibility disks (60 μg/disk) were purchased from Thermo Scientific, Waltham, MA.

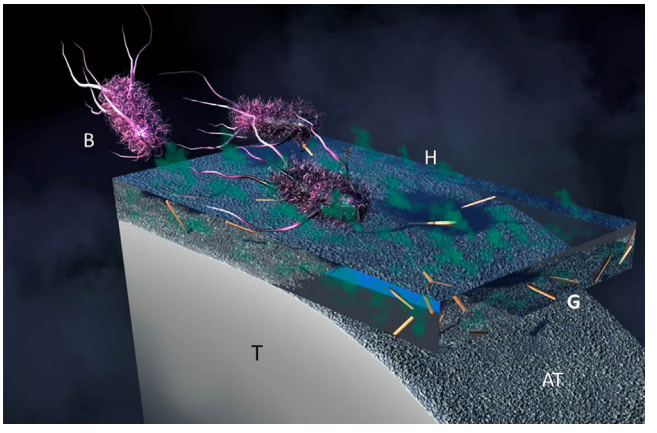

Fig. 1. Graphical representation of the anti-microbial hydrogel (H) coating applied to anodized titanium (AT). From left to right, bacteria (B) encounter the anti-microbial hydrogel and released gentamicin (G) altering their metabolism leading to cell death. T = titanium.

http://dx.doi.org/10.1016/j.heliyon.2016.e00072

2.2. Scanning electron microscopy

Hydrogels were lyophilized in preparation for scanning electron microscopic imaging in order to retain the gel matrix structure. The hydrogel samples were taken out of the autoclaved RO water and placed on Whatman No. 1 filter paper to drain out excess water. These partially dried hydrogels were then frozen in glass beakers at −20 °C overnight before lyophilization. Lyophilization was carried out using a LabConco Lyophilizer for 36 h. The lyophilized hydrogels were then imaged using a HITACHI 4800 Scanning Electron Microscope to reveal details of hydrogel surface. Images were taken at 1 kV and at magnification ranging from 1.00 mm to 100 μm. The control sample was alginate only hydrogel beads. The sample hydrogels consisting: alginate/HNTs, CPC/alginate, and CPC/alginate/chitosan were compared against the control; alginate only hydrogel beads were used as controls for surface morphology analysis.

2.3. Loading of halloysite nanotubes

HNTs were mixed with 50 mg/ml solution of gentamicin sulfate and sonicated continuously for 15 min. Sonicated HNTs were then placed in a vacuum chamber and vacuum was applied for 2 h alternating with vacuum release. This process was carried out for 24 h. The loaded HNTs were then vacuum dried and then given two washes with sterile distilled water to remove traces of Gentamicin sulfate that might have been coated on the HNTs outer surface.

2.4. Elution study for gentamicin from HNTs and hydrogels

The elution data for gentamicin release from HNTs and hydrogels enhanced with HNTs was obtained by studying the release for a period of 24 h. The release was done in simulated body fluid (SBF) buffer (pH 7.5 and temperature ~25 °C). The gentamicin loaded HNTs were mixed with SBF and then samples were collected for fixed time intervals. As GS cannot be detected directly by UV-Visible spectroscopy, an indirect method of detection by ophthalaldehyde reagent was used. This reagent was prepared by adding 250 mg of ophthalaldehyde powder to 6.25 ml of 95% methanol. This mixture was sonicated for 30 min till a clear solution was obtained. 0.3 ml of 2-hydroxy ethyl mercaptan was added to 56 ml of 0.04 M sodium borate and mixed thoroughly. Both these mixtures were added, then sonicated for 15 min before being stored in an amber color container for 24 h. A total of, 1 ml each of collected gentamicin sample, isopropanol (to prevent sedimentation) and ophthalaldehyde reagent were mixed and left undisturbed for 20 min at room temperature. The absorbance for the GS was measured at 333 nm using a Thermo scientific NanoDrop 2000 Spectrophotometer.

http://dx.doi.org/10.1016/j.heliyon.2016.e00072

2.5. Preparation of hydrogels

Sodium alginate (2% w/v) when mixed with calcium chloride (1% w/v) forms a gel matrix by reverse crosslinking. The result is a hydrogel polymer calcium alginate. The calcium alginate hydrogels were enhanced with CPC. In the following compositions, CPC refers to a mixture of tetracalcium phosphate (TTCP) and dicalcium phosphate (DCPA) in 730 mg to 270 mg mixed in equimolar ratios. The formulation for CPC hydrogels with were:

1. CPC/alginate = 1 gm: 3 ml
2. CPC/alginate/chitosan = 1 gm: 20 mg: 6 ml

The hydrogels with CPCs were also enhanced with 1% w/v HNTs to improve their material strength. The control groups have alginate only and alginate + 1% w/v HNTs (Alginate/HNTs) without gentamicin sulfate.

The CPC/alginate and CPC/alginate/chitosan hydrogels were formed by mixing the CPC, chitosan lactate, HNTs and sodium alginate in appropriate proportions and then dropping the mixture in 1% calcium chloride solution using a syringe with 18½ G needle. The hydrogel beads formed instantaneously upon contact with calcium chloride solution but were kept in the solution for complete reverse crosslinking for 15 min. For maintaining hydrated conditions, the hydrogels were stored in RO autoclaved water.

2.6. Bacterial culture

Single colonies of DH5α strain of *E. coli* (lab stock) were cultured in Luria-Bertani (LB) broth liquid medium. The inoculum from the LB broth was plated onto LB agar and Mueller-Hinton plates under sterile conditions.

2.7. Bacterial inhibition studies

Control and experimental hydrogel beads were kept on the inoculated plates and these plates were incubated at 37 °C. These plates were then observed for inhibition zones and compared against gentamicin antimicrobial susceptibility disks.

2.8. Pilot pre-osteoblast study

To assess if the hydrogel coatings would support cell growth and functionality, 3T3 preosteoblasts (ATCC CRL 2593 E1 subclones) were cultured on the coatings. The experimental samples had CPC/alginate, CPC/alginate/chitosan and CPC/alginate/chitosan/HNTs hydrogel films. The objective of this study was to ascertain if the mammalian host tissue cells (3T3 preosteoblasts) can adhere and grow on the hydrogels. If the mammalian cells would adhere or secrete

http://dx.doi.org/10.1016/j.heliyon.2016.e00072

ECM proteins on the hydrogels, this would suggest that the hydrogels support mammalian cell adhesion, growth and functionality and inhibit bacterial growth.

Standard cell culture protocols were followed and sterile conditions maintained throughout the culturing, passaging, seeding and experimental time period. The experimental plates were fixed on days 3, 7, and 14 by adding 95% ethanol. The fixed plates were then stained for ECM proteoglycans, glycoproteins and mucopolysaccharides with Alcian Blue stain and for collagen secretion with Picrosirius Red stain. To quantify the amount of cellular secretions after the cells adhere, the stain was eluted by destaining the plates in 7% v/v acetic acid destaining solution. The destained solution from each well was collected and quantified by UV/Vis spectrophotometry using a NanoDrop 2000 spectrophotometer.

2.9. Statistical analysis

The data from the histochemical analysis (Alcian Blue and Picrosirius Red staining) was plotted as a graph of means of data points per sample/type/day for two experimental trials (n = 3 samples per trial) and the samples were independent of each other. Inferential statistics, such as ANOVA, could not be used because of the limited sample size; hence, a simple descriptive statistic was used for the interpretation of the results. The error bars were calculated as the percent error.

3. Results and discussion

3.1. Surface morphology of hydrogels

Scanning electron microscopy was done on the hydrogel beads to assess the surface morphology of the beads. A comparison between the hydrogels cryo-SEM images revealed that the surfaces of hydrogels with HNTs, CPC, and CPC plus chitosan had a rough and modified surface against a relatively smoother surface of alginate only hydrogel beads as can be seen in Fig. 2 (A–F). The surface topography varied in terms of amplitude and heterogeneity.

The alginate only hydrogels Fig. 2A under cryo-SEM shows a very smooth surface which is almost devoid of any surface features. The alginate only hydrogel shows some elevations which are gentle and some folds which might have resulted because of the process of lyophilization. The hydrogels which are enhanced with other materials like CPC, chitosan, and HNTs have distinctive surface features like ridges, sharp elevations, and depressions. The surface features get formed in the hydrogels because of the interactions of the materials with alginate. Chitosan lactate and HNTs clump in aqueous solutions. In our method of hydrogel preparation, we employed methods to disperse or

http://dx.doi.org/10.1016/j.heliyon.2016.e00072

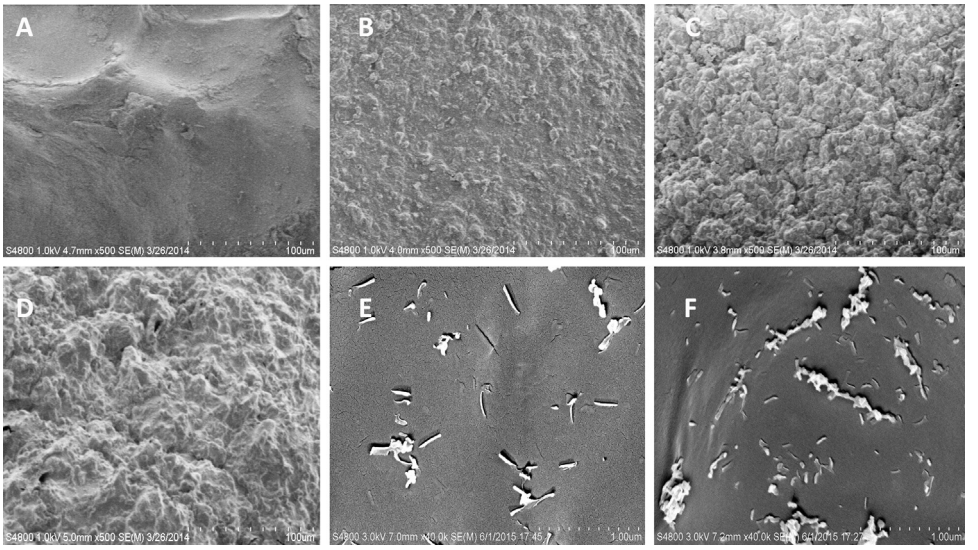

Fig. 2. SEM micrographs of the hydrogel coating surfaces (A) alginate only; (B) alginate/HNTs; (C) CPC/alginate; (D) CPC/alginate/chitosan. At higher magnification, (E and F) HNTs can be seen protruding from the hydrogel surfaces (E) alginate/HNTs; (F) CPC/alginate/HNTs. Scale bar = 100 microns in A to D and 1 micron in E and F.

breakdown these clusters into fine particles and these dispersed particles might give the hydrogels their unique surface topography as seen in the Fig. 2 B–F.

Eukaryotic mammalian cells prefer a relatively rough surface or a surface with some features (heterogeneous) for adherence [40, 41]. Experiments using engineered substrates with nanoscale features have shown the importance of ECM nanotopography on cellular morphology, adhesion, proliferation, and differentiation [40, 41, 42](extensively reviewed in [43, 44]). Zhou et al. [45] showed that on poly(vinyl alcohol) PVA/HNT bionanocomposite surfaces, osteoblasts exhibited a significantly higher level of adhesion than on neat PVA. Accordingly, beads with HNTs, CPC, and chitosan have a rough surface that should be favorable for cell attachment as compared with the smooth alginate only hydrogel surface.

3.2. Gentamicin sulfate release from halloysite nanotubes and hydrogels

Gentamicin sulfate was released from HNTs within a period of 48 h in an experiment samples over 7 days. The graph in Fig. 3 shows that the release obtained is released in a sustained fashion over the 7-day period.

Gentamicin sulfate release from hydrogels was for a period of 5 days (approximately 48 h), in an experiment that took samples over 7 days. The graph in Fig. 4 shows that the release obtained in a sustained fashion for 48 h

http://dx.doi.org/10.1016/j.heliyon.2016.e00072

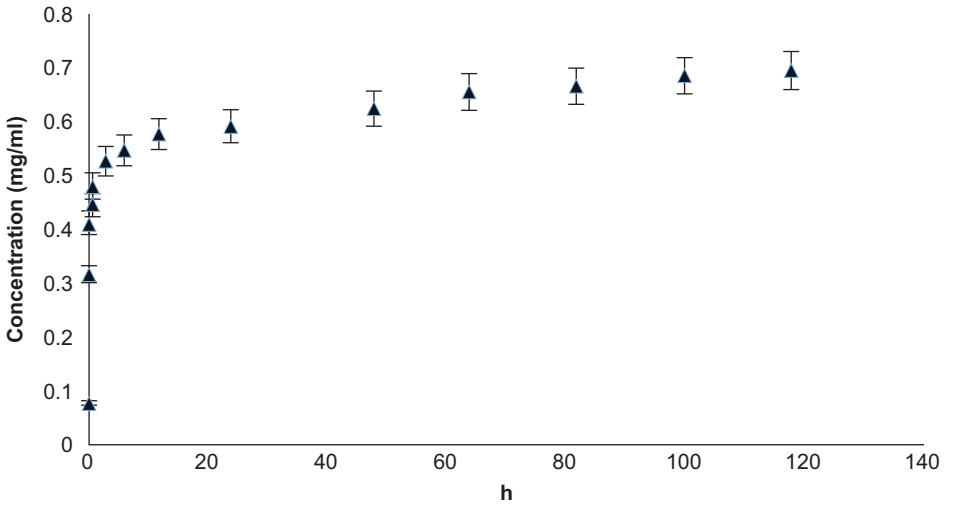

Fig. 3. Cumulative gentamicin sulfate release from HNTs showing time (hours) vs. concentration (mg/ml) (n = 6) with error bars showing percent error (5%).

over the 7-day experimental period. The declining amount of GS that is released from the HNTs cannot be shown in the graph as it is a cumulative release profile. A cumulative plot was chosen to represent the release of gentamicin from HNTs as the amount of drug release at a particular time interval is dependent on the concentration gradient at that particular time point and that in turn is dependent on how much drug is released at a previous time point. However, the authors would like to note here that GS was not detectable after

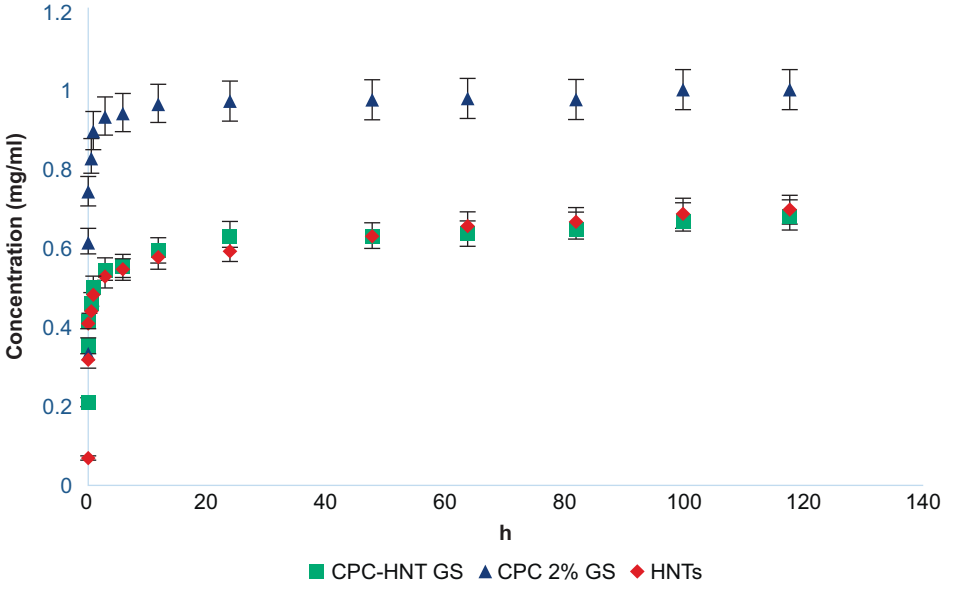

Fig. 4. Cumulative graph of gentamicin sulfate release from hydrogels showing time (hours) vs. concentration (mg/ml) (n = 6) error bars showing percent error (5%).

http://dx.doi.org/10.1016/j.heliyon.2016.e00072

48 h of the experiment suggesting that the gentamicin that was loaded in the HNTs would be exhausted almost entirely or the levels were too low to be detected by the UV/Vis spectrometry.

The groups studied for the release of GS in Fig. 4 are CPC-1% w/v HNTs + GS (shown by green square), CPC with 2% v/v GS directly loaded in the CPC (blue triangle), and HNTs with GS (red diamond). The graph shows the release kinetics of the GS from these various groups from the HNTs or the hydrogel directly in pH 7 at room temperature. The curve shows the release of GS that is adsorbed on the surface of the HNTs as well as the molecules that have been loaded inside the lumen of the HNTs.

The maximum loading efficiency of HNTs is about 12% of its volume [59]. The ability of HNTs to encapsulate and provide sustained release has been demonstrated for a variety of chemical agents, including antiseptics and antibacterials [46, 47, 48], drugs [49, 50] growth factors [51, 52] and DNA [53]. In the majority of studies, encapsulation in halloysite significantly reduced drug release and in the case of BMP-2 (51) allowed release of this growth factor in picogram range.

Gentamicin-doped HNTs were embedded in poly methyl-methacrylate (PMMA) beads and PMMA bone cement. Gentamicin and other antibiotics have been added to cement to improve local antibiotic delivery in addition to intravenous or oral doses [39, 53, 54, 55, 56]. Commercial-grade PMMA bone cement formulations release 70% of gentamicin within the first 24 h [54, 55]. Wei et al. [54] showed that PMMA bone cement doped with gentamicin loaded halloysite nanotubes released gentamicin in a slow and sustained fashion and did not compromise composite mechanical strength [54].

In case of GS, the molecule size is relatively smaller when compared to the HNTs. Gentamicin sulfate used in this study is in solution form and the molecules would adhere on all the surfaces of the HNTs. The elution patterns shown in Fig. 3 and Fig. 4 show the possible adsorption patterns on both the inner and outer surfaces. The initial burst release may be due to the molecules that have adhered to the outer surface of the HNTs and desorb faster as compared to the molecules loaded inside the tubes. The extended release of the drug can be attributed to the slow desorption of the molecules that are loaded in the inner lumen of the HNTs. Drug release from the lumen is a slow process as it involves several steps: solvent diffusion into the lumen, drug diffusion in the solvent in the lumen followed by the diffusion of drug from solvent in the lumen in to the surrounding solution. As the solvent can only diffuse into the lumen from the pores (two ends of the nanotube), elution from the lumen may be delayed to an extended period.

 http://dx.doi.org/10.1016/j.heliyon.2016.e00072

3.3. Bacterial study

Having shown that our hydrogel coatings can release gentamicin in the range of 0.5–1 mg/ml we initiated a bacterial study using hydrogels, with and without gentamicin sulfate loaded halloysite, conducted on Mueller-Hinton agar plates cultured with *E. coli*. The plates were observed after 24 h of incubation at 37 °C. The positive control had a uniform deposition of *E. coli* growth and the negative control showed no bacteria growth on it as seen in Fig. 5A and B.

Hydrogels enhanced with the HNTs but without being doped with gentamicin sulfate were placed on the Mueller-Hinton agar plates with *E. coli*. After 24 h, no zones of inhibition were observed on the plates as can be seen in Fig. 6 suggesting that the hydrogels themselves are not anti-microbial.

The hydrogels with gentamicin sulfate loaded HNTs produced extensive zones of growth inhibition as seen in Fig. 7C and D that are comparable with the gentamicin control disks. The zones of inhibition on the plates with gentamicin loaded HNT- hydrogels indicate that the anti-bacterial agent released from the hydrogels is capable of inhibiting the growth of bacteria on the agar plates. The zones of inhibition in all of these plates, Fig. 6 II–IV, have an average diameter of approximately 1 cm. This can prevent the formation of bacterial colonies and in turn bacterial films on the implant surface in turn increasing the chances of infection free implant.

That these hydrogels have antimicrobial properties would suggest that these hydrogel coatings on implants will decrease the chance of post-surgical infection. The experiment was conducted for a 7-day period but the gentamicin was released in 48 h. The points after 48 h show a plateau.

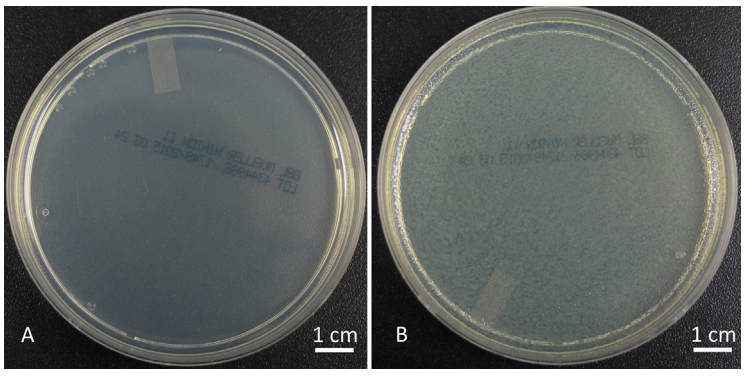

Fig. 5. (A) Negative control Mueller-Hinton plate and (B) Positive control Mueller-Hinton plate with *E. coli* colonies. (–ve = negative control, +ve = positive control, n = 6).

http://dx.doi.org/10.1016/j.heliyon.2016.e00072

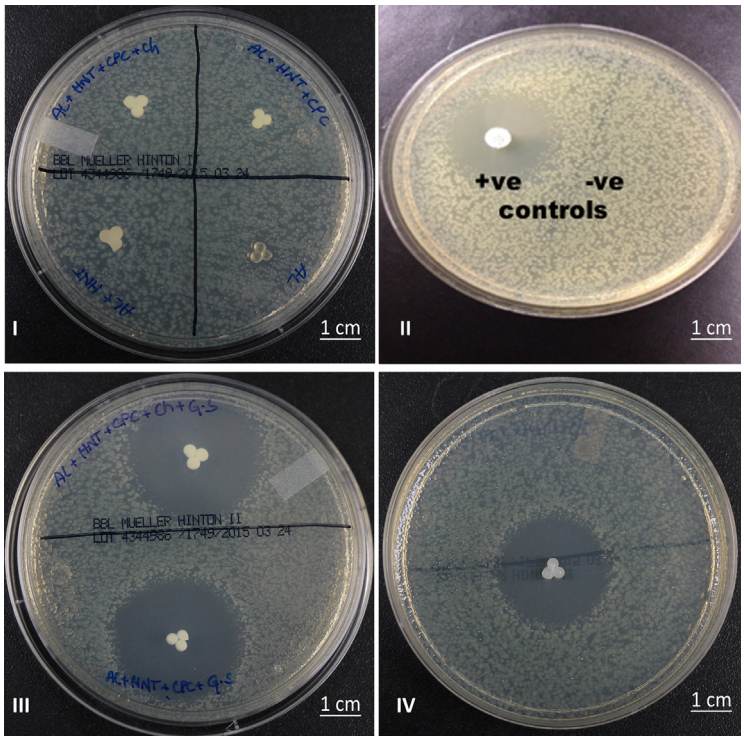

Fig. 6. Bacterial growth inhibition studies. (I) (a) Alginate + HNTs + CPC + chitosan, (b) Alginate + HNTs + CPC, (c) Alginate only, and (d) Alginate + HNTs. (II) (a) Gentamicin control disk (60 mg gentamicin) shows a large zone of inhibition. (b) *E. coli* growing as a continuous lawn. (III) Mueller-Hinton plate with hydrogels with gentamicin sulfate showing zones of inhibition (top) alginate + HNTs + CPC + chitosan + gentamicin, (bottom) alginate + HNTs + CPC + gentamicin, (IV) alginate + HNTs + gentamicin (n = 6).

3.4. Pre-osteoblast pilot study

A pilot study was conducted to identify the hydrogel coating that best supports cell viability and growth. The response of NIH 3T3 pre-osteoblasts after culture upon calcium alginate and calcium phosphate cement (CPC) hydrogel composites, with and without HNTs, was assessed through histochemical staining for detection of collagen and proteoglycan synthesis. For proteoglycan detection, the stain Alcian Blue was used. After each coating was stained, the dye was eluted with a 7% v/v acetic acid destaining solution and quantified by spectrophotometry. An indirect method of quantification was used instead of a conventional staining and imaging approach as the scaffold films were too thick for conventional light microscopy to photodocument cells attached to the coatings. The difference in acidic polysaccharides secreted by the cells adhered to the coatings is expressed as absorbance vs. days in culture (Fig. 8). The study was conducted using triplicates of each sample and repeated twice to check the reproducibility of results.

http://dx.doi.org/10.1016/j.heliyon.2016.e00072

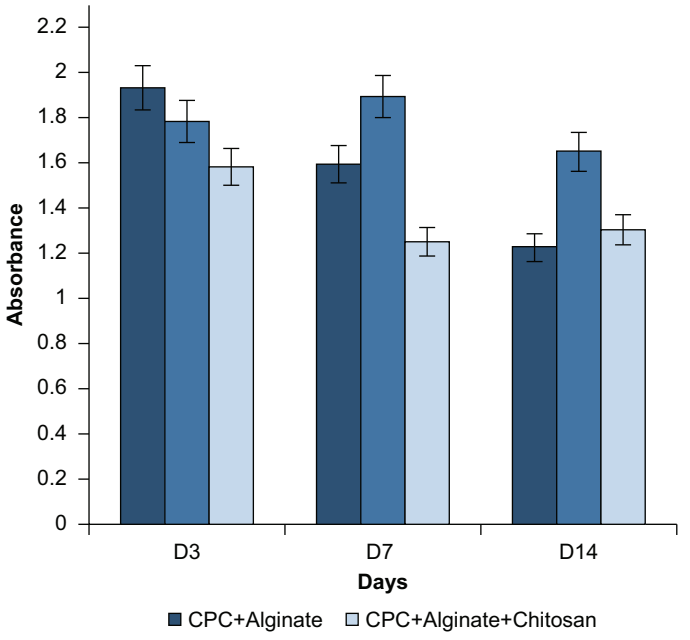

Fig. 7. Graph showing the absorbance (at 450-495 nm) of the eluted Alcian Blue stain against the number of days and different hydrogel composition (n = 6).

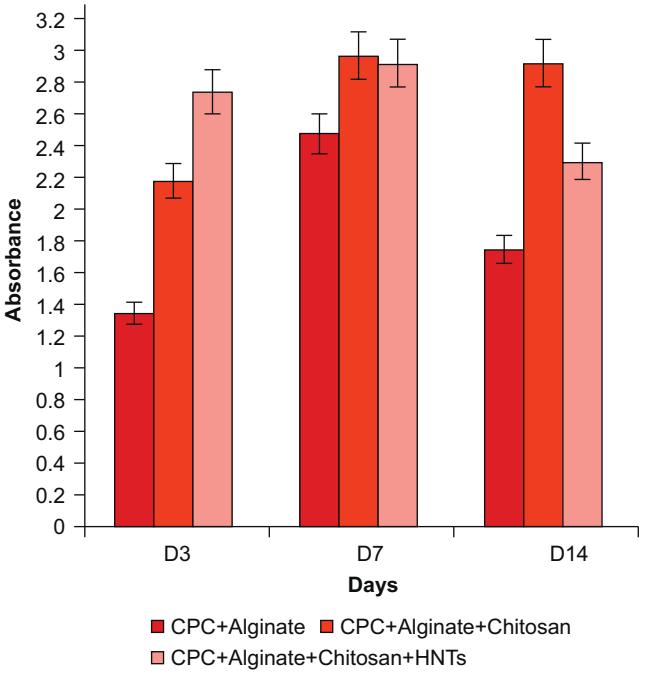

Fig. 8. Graph showing the absorbance (at 620–750 nm) of the eluted Picrosirius Red stain against the number of days (n = 6).

http://dx.doi.org/10.1016/j.heliyon.2016.e00072

Alcian Blue staining results shows that the CPC/alginate films had synthesized a greater amount of proteoglycan day 3 but there was a drop by day 14. The CPC/alginate films also had comparatively more sulfated ECM than the rest of the films as shown in Fig. 7 on day 3. The CPC/alginate/chitosan films maintained sulfated ECM levels relatively equal on days 3, 7 and 14. The CPC/alginate/chitosan/HNTs films had the least sulfated ECM on day 3 when compared against the other scaffolds. The levels of sulfated ECM decreased on day 7 but remained relatively similar on day 14.

To quantify collagen secretion, the Picrosirius Red stain was used to stain cells on hydrogel coatings. Osteoblasts produce an organic matrix, principally composed of type I collagen (Osteoid) prior to its mineralization. After destaining in 7% v/v acetic acid, the eluted stain was quantified through UV/Vis spectrophotometry. The results are shown in Fig. 8 as collagen secreted by adherent cells as absorbance plotted against number of days in culture.

Picrosirius Red staining data showed that the CPC/alginate films had accumulated the less amount of collagen on day 3 but increased by day 7 with a decrease noted on day 14. The CPC/alginate films also had produced a lesser amount of collagen when compared with the other two coatings (Fig. 8) In contrast, CPC/alginate/chitosan films produced an initial higher amount of collagen which was maintained through day 14. CPC/alginate/chitosan/HNT films produced the most collagen by day 3 when compared against the other scaffolds. The levels of collagen remained relatively similar on days 3 and 7 and decreased in amount by day 14. The cumulative supports the observation that cells on all substrates produced a base organic extracellular matrix.

When we reviewed the histochemical staining data, we observed a relationship between the amount of ECM proteoglycans and collagen secreted by cells throughout the 14 day period. CPC/alginate films had accumulated a more proteoglycan-rich matrix by day 3 but the synthesis of collagen was reduced when compared with the other hydrogel types. The CPC/alginate/chitosan/HNTs hydrogel coatings showed the least production of proteoglycan by day 3 by comparison but assembled a more collagen-rich matrix when compared against the other hydrogel coatings. Therefore, the two formulations that hold the most promise for tissue formation are CPC + Alginate + Chitosan and CPC + Alginate + Chitosan + HNTs.

We used a descriptive statistic in this study that explained the qualitative significance of the data. The samples were independent of each other and the values reflect the averages of the readings that were taken per sample for that particular day in two separate trials. When considering the matrix production of cells cultured on each hydrogel coating, the most cell supportive hydrogel type was CPC/alginate/chitosan with both proteoglycan and collagen synthesis

http://dx.doi.org/10.1016/j.heliyon.2016.e00072

remaining relatively stable on all the days. The CPC/alginate/chitosan and CPC/alginate/chitosan/HNT hydrogel film synthesized greater amounts of ECM proteins throughout the 14-day period with respect to proteoglycan and collagen secretion. Both hydrogel types produced comparable amounts of proteoglycan and collagen on days 7 and 14.

5. Conclusions

The anti-microbial agent, gentamicin sulfate, was released from halloysite nanoclay and from hydrogels enriched with this nanoclay for a period of 5 days. The pattern of gentamicin sulfate release from the nanoclay-enriched hydrogels supplied anti-microbial agents in a sustained manner. The released gentamicin sulfate showed that it inhibits the growth of *E. coli* on Mueller-Hinton plates for 24 h similar to the gentamicin sulfate antimicrobial susceptibility disks (10 μg/disk). The first 24 h after the surgical implantation of any implant are crucial and if infection does not set in within these 24 h then chances for implant stability and acceptance should increase. The pilot cell study using 3T3 preosteoblasts also suggest that the hydrogel coatings will provide a suitable and cell supportive implant surface for mammalian cells.

Declarations

Author contribution statement

Sonali Karnik: Conceived and designed the experiments; Performed the experiments; Analyzed and interpreted the data; Wrote the paper.

Udayabhanu M. Jammalamadaka, Karthik K. Tappa: Performed the experiments; Analyzed and interpreted the data.

Becky Girono: Analyzed and interpreted the data; Contributed reagents, materials, analysis tools or data; Wrote the paper.

David K. Mills: Conceived and designed the experiments; Analyzed and interpreted the data; Wrote the paper.

Funding statement

Dr. David K. Mills was supported by a grant from the Louisiana Governor's Biotechnology Initiative.

Competing interest statement

The authors declare no conflict of interest.

http://dx.doi.org/10.1016/j.heliyon.2016.e00072

Additional information

No additional information is available for this paper.

Acknowledgments

The authors would like to thank Dr. Alfred Gunasekaran for his help in the scanning electron microscopy of the hydrogel samples. We would like to thank Mr. Chris Boyer, Nano Developments LLC., LA, for the graphical representation in Fig. 1.

References

[1] M. Long, H.J. Rack, Titanium alloys in total joint replacement – a materials science perspective, Biomaterials 19 (1998) 1621–1639.

[2] S.B. Goodman, Y. Zhenyu, M. Keeney, F. Yang, The future of biologic coatings for orthopaedic implants, Biomaterials 34 (2013) 3174–3183.

[3] S. Weerachai, Biological Responses to New Advanced Surface Modifications of Endosseous Medical Implants, Bone and Tissue Regeneration Insights 2 (2009) 1–11.

[4] Medical Device Coatings Market - Global Industry Size, Share, Trends, Analysis And Forecasts 2012–2018. http://www.transparencymarketresearch.com/medical-device-coatings-market.html#sthash.O0tJiX0F.dpuf Accessed on February 16, 2014.

[5] The Global Joint Arthroplasty and Orthopedic Bone Cement Market Report. (2012) Orthopedic Network News, 23(4), October 2012. Accessed on February 16, 2014.

[6] S.L. Assis, S. Wolynec, I. Costa, Corrosion characterization of titanium alloys by electrochemical techniques, Electrochim. Acta 51 (2006) 1815–1819.

[7] C.E. Wen, Y. Yamada, K. Shimojima, Y. Chino, et al., Processing and mechanical properties of autogenous titanium implant materials, J. Mater. Sci. Mater. M. 13 (2002) 397–401.

[8] M. Geetha, A.K. Singh, R. Asokamani, A.K. Gogia, Ti based biomaterials, the ultimate choice for orthopaedic implants–A review, Prog. Mater. Sci. 54 (2009) 397–425.

[9] M. Niinomi, Mechanical biocompatibilities of titanium alloys for biomedical applications, J. Mech. Behav. Biomed. 1 (2008) 30–42.

 http://dx.doi.org/10.1016/j.heliyon.2016.e00072

[10] Y. Zhao, T. Xiong, W. Huang, Effect of heat treatment on bioactivity of anodic titania films, Appl. Surf. Sci. 256 (2010) 3073–3076.

[11] E.M. Hetrick, M.H. Schoenfish, Reducing implant-related infections: active release strategies, Chem. Soc. Rev. 2006 (35) (2006) 780–789.

[12] J. Hardes, H. Ahrens, C. Gebert, A. Streitbuerger, H. Buerger, M. Erren, et al., Lack of toxicological side-effects in silver-coated megaprostheses in humans, Biomaterials 28 (2006) 2869–2875.

[13] L.Z. Zhao, H.R. Wang, K.F. Huo, L.Y. Cui, W.R. Zhang, H.W. Ni, et al., Antibacterial nano-structured titania coating incorporated with silver nanoparticles, Biomaterials 32 (2012) 5706–5716.

[14] P. Lichtea, P. Kobbea, D. Dombroskib, H.C. Papea, Damage control orthopedics: current evidence, Curr. Opin. Crit. Care 18 (2012) 647–650.

[15] Orthopedic Bone Cement and Casting Materials Market Outlook in BRICS (Brazil, Russia, India, China, South Africa) to 2018. http://www.researchandmarkets.com/reports/2228361/ Accessed on February 16, 2014.

[16] R. Torrecillas, J.S. Moya, L.A. Diaz, J.F. Bartolome, A. Fernandez, S. Lopez-Esteban, Nanotechnology in joint replacement, Nanomed. Nanobiotechnol. 1 (2009) 540–552.

[17] N. Harrison, P.E. McHugh, W. Curtin, P. McDonnell, Micromotion and friction evaluation of a novel surface architecture for improved primary fixation of cementless orthopaedic implants, J. Mech. Behav. Biomed. Mater. 21 (2013) 37–46.

[18] N.J. Hickok, I.M. Shapiro, Immobilized antibiotics to prevent orthopaedic implant infections, Adv. Drug Deliv. Rev. 64 (2012) 1165–1176.

[19] R.O. Darouiche, Treatment of infections associated with surgical implants, N. Engl. J. Med. 350 (2004) 1422–1429.

[20] P.S. Stewart, J.W. Costerton, Antibiotic resistance of bacteria in biofilms, The Lancet 358 (2001) 135–138.

[21] P. Stoodley, K. Sauer, D.G. Davies, J.W. Costerton, Biofilms as complex differentiated communities, Annu. Rev. Microbiol. 56 (2002) 187–209.

[22] E.J. McPherson, C. Woodson, P. Holtom, N. Roidis, C. Shufelt, M. Patzakis, Periprosthetic total hip infection: outcomes using a staging system, Clin. Orthop. Relat. Res. 403 (2002) 8–15.

 http://dx.doi.org/10.1016/j.heliyon.2016.e00072

[23] L. Pulido, E. Ghanem, A. Joshi, J.J. Purtill, J. Parvizi, Periprosthetic joint infection: the incidence, timing, and predisposing factors, Clin. Orthop. Relat. Res. 466 (2008) 1710–1715.

[24] G. Cierny , D. DiPasquale, Periprosthetic total joint infections: staging, treatment, and outcomes, Clin. Orthop. Relat. Res. 403 (2002) 23–28.

[25] B. Fink, A. Grossmann, M. Fuerst, P. Schafer, L. Frommelt, Two-stage cementless revision of infected hip endoprostheses, Clin. Orthop. Relat. Res. 467 (2009) 1848–1858.

[26] Y.H. Zheng, J.B. Li, X.Y. Liu, J. Sun, Antimicrobial and osteogenic effect of Ag-implanted titanium with a nanostructured surface, Int. J. Nanomedicine 7 (2012) 875–884.

[27] M. Shenghin, H. Wang, W. Wang, L. Tong, H. Pab, et al., Antibacterial effects and biocompatibility of titanium surfaces with graded silver incorporation in titania nanotubes, Biomaterials 35 (2014) 4255–4265.

[28] M.W. Chang, S.S. Jeong, X. Qi, A.R. Sharif, et al., A photopolymerized antimicrobial hydrogel coating derived from epsilon-poly-L-lysine, Biomaterials 32 (2011) 2704–2712.

[29] L.Z. Zhao, P.K. Chu, Y.M. Zhang, Z.F. Wu, Antibacterial coatings on titanium implants, J. Biomed. Mater. Res. B 91B (2009) 470–480.

[30] L.G. Harris, S. Tosatti, M. Wieland, M. Textor, R.G. Richards, Staphylococcus aureus adhesion to titanium oxide surfaces coated with non-functionalized and peptide-functionalized poly(L-lysine)-grafted-poly (ethylene glycol) copolymers, Biomaterials 25 (2004) 4135–4148.

[31] M.L.W. Knetsch, L.H. Koole, New strategies in the development of antimicrobial coatings: The example of increasing usage of silver and silver nanoparticles, Polymers 3 (2011) 340–366.

[32] L. Ge, Q. Li, M. Wang, X. Qouyang, M. Xing, Nanosilver particles in medical applications: synthesis, performance, and toxicity, Int. J. Nanomedicine 9 (2014) 2399–2407.

[33] S.B. Goodman, Y. Zhenyu, M. Keeney, F. Yang, The future of biologic coatings for orthopaedic implants, Biomaterials 34 (2013) 3174–3183.

[34] S. Weerachai, Biological responses to new advanced surface modifications of endosseous medical implants, Bone and Tissue Regeneration Insights 2 (2009) 1–11.

 http://dx.doi.org/10.1016/j.heliyon.2016.e00072

[35] G.A. Crawford, N. Chawla, K. Das, S. Bose, A. Bandyopadhyay, Microstructure and deformation behavior of biocompatible TiO2 nanotubes on titanium substrate, Acta Biomater. 3 (2007) 359–367.

[36] J. Park, S. Bauer, K. von der Mark, P. Schmuki, Nanosize and vitality: TiO2 nanotube diameter directs cell fate, Nano Lett. 7 (2007) 1686–1691.

[37] J. Howard, S. Patel, D.K. Mills, S. Gold, Assessment of cell-material interactions on 3D nanostructured titania-polymer surfaces towards the improvement of osseointegration of orthopedic and dental implants, Paper No. 166C presented at the American Institute of Chemical Engineers, Philadelphia, PA, (Nov. 2008), 2008.

[38] S. Patel, D.K. Mills, J. Howard, Y. Lvov, Surface modification of metallic implants to enhance osteogenesis, FASEB J. 23 (2009) 647.7.

[39] S. Tsourvakas, Local antibiotic therapy in the treatment of bone and soft tissue infections, In: S. Danilla (Ed.), Selected Topics in Plastic Reconstructive Surgery, InTech, Dubrovnik, Croatia, 2012.

[40] T.W. Chung, D.Z. Liu, S.Y. Wang, S.S. Wang, Enhancement of the growth of human endothelial cells by surface roughness at nanometer scale, Biomaterials 24 (25) (2003) 4655–4661.

[41] R.A. Gittens, T. McLachlan, R. Olivares-Navarrete, Y. Cai, S. Berner, R. Tannenbaum, Z. Schwartz, K.H. Sandhage, B.D. Boyan, The effects of combined micron-/submicron-scale surface roughness and nanoscale features on cell proliferation and differentiation, Biomaterials 32 (13) (2011) 3395–3403.

[42] T.S. Silva, D.C. Machado, C. Viezzer, A.N. Silva , M.G. Oliveira, Effect of titanium surface roughness on human bone marrow cell proliferation and differentiation: an experimental study, Acta Cir. Bras. 3 (2009) 200–205.

[43] K. Deok-Ho, P. Paolo, C.L. Smith, A.J. Levchenko, Matrix nanotopography as a regulator of cell function, Cell Biol. 197 (2012) 3351–3360.

[44] M.J. Dalby, N. Gadegaard, O.C. Richard, R. Oreffo, Harnessing nanotopography and integrin–matrix interactions to influence stem cell fate, Nat. Mater. 13 (6) (2014) 558–569.

[45] W.Y. Zhou, B. Guo, X. Liu, R. Liao, A.B. Rabie, D. Jia, Poly(vinyl alcohol)/halloysite nanotubes bionanocomposite films: Properties and in vitro osteoblast and fibroblast response, J. Biomed. Mater. Res. A 93 (4) (2010) 1574–1587.

 http://dx.doi.org/10.1016/j.heliyon.2016.e00072

[46] W. Wei, R. Minullina, E. Abdullayev, R. Fakhrullin, D.K. Mills, Y.M. Lvov, Enhanced efficiency of antiseptics with sustained release from clay nanotubes, RSC Adv. 4 (2014) 485–488.

[47] R. Qi, R. Guo, M. Shen, X. Cao, L. Zhang, J. Xu, J. Yu, X. Shi, Electrospun poly(lactic-co-glycolic acid)/halloysite nanotube composite nanofibers for drug encapsulation and sustained release, J. Mat. Chem. B 20 (47) (2010) 10622–10629.

[48] K. Tappa, U. Jammalamadaka, D.K. Mills, Conference: 36th Annual IEEE-EMBS Conf., 2014, Design and Evaluation of a Nanoenhanced Anti-Infective Calcium Phosphate Bone Cement, 7592014, pp. 1–4.

[49] L. Fan, B. Li, Q. Wang, A. Wang, W. Zhang, Superhydrophobic gated polyorganosilanes/halloysite nanocontainers for sustained drug release, Adv. Mat. Interfac. 1 (5) (2014) 1–7.

[50] D. Shchukin, R. Price, Y. Lvov, Biomimetic synthesis of vaterite in the interior of clay nanotubules, Small 1 (2005) 510–513.

[51] S. Karnik, K. Hines, D.K. Mills, Nanoenhanced hydrogel system with sustained release capabilities, J. Biomed. Mater. Res. Part A 103A (2015) 2416–2426.

[52] U. Jammalamadaka, K. Tappa, D.K. Mills, 36th Annual IEEE EMBS Conference., Osteoinductive calcium phosphate clay nanoparticle bone cements (CPCs) with enhanced mechanical properties, 7592014, pp. 1–4.

[53] M.H. Shamsi, K.E. Geckeler, The first biopolymer-wrapped non carbon nanotubes, e-Nanotech 19 (2008) 1–5.

[54] W. Wei, E. Abdllayev, A. Goeders, A. Hollister, D.M. Lvov, D.K. Mills, Clay nanotube/poly(methyl methacrylate) bone cement composite with sustained antibiotic release, Macromol. Mat. Eng. 297 (2012) 645–653.

[55] M. Virto, P. Frutos, S. Torrado, G. Frutos, Gentamicin release from modified acrylic bone cements with lactose and hydroxypropylmethylcellulose, Biomaterials 24 (2003) 79–87.

[56] Y. Chang, C.L. Tai, H. Hsieh, S.W.N. Ueng, Gentamicin in bone cement, Bone Joint Res. 2 (10) (2013) 220–226.

[57] E. Hope, J. Kittrick, Surface tension and the morphology of halloysite, Amer. Miner. 49 (1964) 859–863.

 http://dx.doi.org/10.1016/j.heliyon.2016.e00072

[58] E. Joussein, S. Petit, J. Churchman, B. Theng, D. Righi, B. Delvaux, Halloysite clay minerals — a review, Clay Miner. 40 (2005) 383–426.

[59] N. Veerabadran, R. Price, Y. Lvov, Clay nanotubes for encapsulation and sustained release of drugs, Nano 02 (02) (2007) 115–120.

http://dx.doi.org/10.1016/j.heliyon.2016.e00072